Available online at www.sciencedirect.com

SciVerse ScienceDirect

Acta Materialia 59 (2011) 6963–6974

Acta MATERIALIA

www.elsevier.com/locate/actamat

# Comparison of atomistic and elasticity approaches for carbon diffusion near line defects in α-iron

R.G.A. Veiga [a,*], M. Perez [a,1], C.S. Becquart [b,c], E. Clouet [d], C. Domain [e,c]

[a] Université de Lyon, INSA Lyon, Laboratoire MATEIS, UMR CNRS 5510, 25 Avenue Jean Capelle, F69621, Villeurbanne, France
[b] Unité Matériaux et Transformations (UMET), Ecole Nationale Supérieure de Chimie de Lille, UMR CNRS 8207, Bat. C6, F59655 Villeneuve d'Ascq Cedex, France
[c] Laboratoire commun EDF-CNRS Etude et Modélisation des Microstructures pour le Vieillissement des Matériaux (EM2VM), France
[d] Service de Recherches de Métallurgie Physique, CEA/Saclay, 91191 Gif-sur-Yvette, France
[e] EDF, Recherche et Développement, Matériaux et Mécanique des Composants, Les Renardières, F77250 Moret sur Loing, France

Received 6 May 2011; received in revised form 17 July 2011; accepted 21 July 2011
Available online 26 August 2011

**Abstract**

Energy barriers for carbon migration in the neighborhood of line defects in body-centered cubic iron have been obtained by atomistic simulations. For this purpose, molecular statics with an Fe–C interatomic potential, based on the embedded atom method, has been employed. Results of these simulations have been compared to the predictions of anisotropic elasticity theory. The agreement is better for a carbon atom sitting on an octahedral site (energy minimum) than one on a tetrahedral site (saddle point). Absolute differences in the energy barriers obtained by the two methods are usually below 5 meV at distances larger than 1.5 nm from a screw dislocation and 2 nm (up to 4 nm in the glide plane) from the edge dislocation. Atomistic kinetic Monte Carlo simulations performed at $T = 300$ K and additional analysis based on the activation energies obtained by both methods show that they are in good qualitative agreement, despite some important quantitative discrepancies due to the large absolute errors found near the dislocation cores.


*Keywords:* Dislocations; Strain aging; Anisotropic elasticity; Atomistic simulations; Kinetic Monte Carlo

## 1. Introduction

The interaction of impurities, notably carbon, with dislocations has long been known to have an important role in the mechanical properties of steels. According to the pioneering work by Cottrell and Bilby [1], during strain aging, carbon atoms in solid solution in the iron matrix are dragged by the long-range stress field of dislocations. When carbon atoms are trapped by a dislocation, the dislocation itself becomes pinned and in order to make it move a larger external stress has to be applied. Aside from increasing the yield strength of steel [2], dislocation pinning causes effects such as the creation of Lüders bands or Portevin–LeChatelier strain localization phenomena [3,4].

The kinetics of phenomena ruled by rare events, such as carbon diffusion in body-centered cubic (bcc) iron, can be satisfactorily described by a series of long stays in stable states punctuated by sudden jumps over energy barriers. Some algorithms used in computer simulations (e.g. kinetic Monte Carlo [5–8]) take advantage of this description to reach time scales not accessible by a method like molecular dynamics. In order to employ transition discretization methods, like kinetic Monte Carlo, the energies of the stable states (local energy minima in the potential energy surface) and the saddle points have to be evaluated. The potential energy barrier, or activation energy, to be surpassed is the difference between those energies. Both the time the system will reside in a stable state and the probability that it will undergo one of the allowed

* Corresponding author. Tel./fax: +33 4 7243 8539.
*E-mail address:* rgaveiga@gmail.com (R.G.A. Veiga).
[1] On sabbatical leave at the Department of Materials Engineering at University of British Columbia, Vancouver, Canada.

1359-6454/$36.00 © 2011 Acta Materialia Inc. Published by Elsevier Ltd. All rights reserved.
doi:10.1016/j.actamat.2011.07.048

transitions, according to the transition state theory [9–11], can be related to the barrier height of those transitions.

Energy barriers for transitions at the atomic scale can be obtained by atomistic simulations that mimic the true chemical environment by employing some simplified description of the atomic interactions involved. Such an approach represents an extraordinary gain in computational time compared to state-of-the-art density functional theory (DFT) calculations that explicitly take into account the electronic structure contribution. Nonetheless, depending on the system size and number of simulations, computational time remains an issue. It has recently been shown that the results of anisotropic elasticity theory compare well to atomistic simulations of the interaction of vacancies with an edge dislocation in fcc metals [12]. Clouet and co-workers have also reported a close agreement between the carbon–dislocation binding energies obtained by atomistic simulations and anisotropic elasticity theory [13]. More recently, Hanlumyuang and co-workers modeled carbon distribution and concentration around dislocations in bcc iron with a combination of DFT and elasticity calculations. They concluded that the effects of chemistry and magnetism beyond those already reflected in the elastic constants can be safely ignored [14]. Taken together, these studies provide evidence that elasticity theory can accurately describe the interaction of point and line defects provided that they are separated by a minimum distance to be determined on a case-by-case basis. In this paper, we present atomistic simulations and calculations based on anisotropic elasticity theory that predict energy barriers for carbon migration in the vicinity of dislocations in α-iron. The aim is to assess the extent to which carbon diffusion in a bcc Fe lattice strained by the presence of dislocations can be described purely by the elastic interactions between the point and the line defects.

## 2. Theoretical and computational approach

### 2.1. Atomistic simulations

The atomistic (molecular statics) simulations presented in this work were performed by LAMMPS [15] with an interatomic potential built according to the embedded atom method (EAM) proposed by Daw and Baskes [16]. Fe–C interactions are described by the Becquart–Raulot potential [17], whereas the Fe–Fe part was developed by Mendelev et al. [18]. It should be mentioned that an incorrect description of the potential energy landscape around the saddle point was recently solved by modifying the Fe–C pairwise interaction function,[2] so that the EAM potential employed in this work is not exactly the same as the one used in Refs. [19,13,20]. This modification has no noticeable effect on the energy minimum corresponding to a C atom occupying an octahedral site.

The simulation boxes employed in this study are depicted in Fig. 1. They consisted of cylinders of radius 15 nm with either an edge or a screw dislocation in the center. The dislocation lines were parallel to the cylinder axis. Periodic boundary conditions were only applied along the dislocation lines. A 2 nm thick (about five times the potential cutoff) outer shell of iron atoms (represented by the green rings in Fig. 1) was kept fixed in the simulations, in order to avoid spurious relaxation of the free surfaces and thus permanently represent the displacement field of the dislocation far away from the dislocation line. The iron atoms have been arranged on a bcc lattice with $a_0 = 0.28553$ nm, i.e. the equilibrium lattice parameter given by the EAM potential. Both dislocations have been created by displacing the iron atoms according to the anisotropic elasticity theory of straight line defects [21–23]. Such a displacement corresponds to the Volterra elastic field created by the dislocation. In both cases, the Burgers vector is $\vec{b} = a_0/2[1\,1\,1]$ and the glide plane is the $\{\bar{1}\,0\,1\}$ plane. These dislocations are the most commonly observed in α-iron. For the edge dislocation, the dislocation line is oriented along the $[1\,\bar{2}\,1]$ direction, whereas the dislocation line for the screw dislocation is oriented along the $[1\,1\,1]$ direction.

In a strain-free α-iron crystal, a carbon atom is found in an octahedral (O) site, which is located in the middle of one of the three edges of the cubic unit cell. Considering the orientation of the two iron atoms that are the first nearest neighbors of the carbon atom, there are three equivalent variants of the octahedral sites along either the [1 0 0], [0 1 0], or [0 0 1] directions. Obviously, this equivalence is lost even at a low strain level, but provided that the strain is not too high, the O-sites remain the energy minima. A carbon atom migrates from an O-site to one of its four neighboring O-sites passing through a tetrahedral (T) site (the saddle point) located at the middle of the minimum energy path [24,25]. A T-site can be associated with the direction defined by two neighboring O-sites. For instance, a carbon atom occupying a [1 0 0] O-variant can jump either to a [0 1 0] or to a [0 0 1] O-variant (there are two of each as nearest neighbors). In the first case, the initial and final O-sites are aligned in the [0 0 1] direction, therefore the T-site between them is labeled [0 0 1] T-variant. The same reasoning has been used to define the [1 0 0] and [0 1 0] tetrahedral variants.

The binding energy of a carbon atom occupying either an octahedral or a tetrahedral site to a dislocation, obtained from atomistic simulations, can be defined as:

$$E^{b}_{[O|T],atom} = E_{[O|T],carbon} + E_{dislo} - E_{[O|T],carbon+dislo} \quad (1)$$

In Eq. (1), $E_{O,carbon} = -10.059$ eV and $E_{T,carbon} = -9.243$ eV are the energies added by an isolated carbon atom occupying an O- or a T-site in α-iron, respectively, according to the interatomic potential. These energies can

[2] Three gaussian functions $g_i(r) = a_i \exp[-(r - r_i)^2/60\sigma]$ were added to the Fe–C pairwise interaction function near $r = 0.257$ nm in order to lower the second derivative. This brings the saddle point back to the tetrahedral site (the original EAM potential predicts in fact four degenerate saddle points located at 0.02 nm from the T-site), in better agreement with ab initio calculations. The values of the parameters are: $a_1 = -0.01$, $a_2 = a_3 = 0.01$, $r_1 = 0.2539$ nm, $r_2 = 0.2365$ nm, $r_3 = 0.2713$ nm, and $\sigma = 0.0002$.

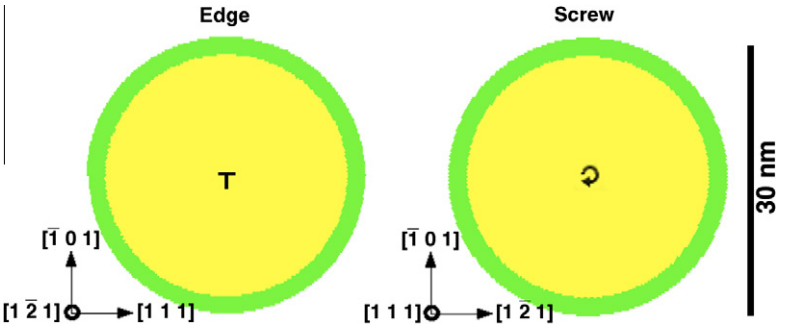


Fig. 1. Top view of the cylindrical simulation boxes containing either an edge or a screw dislocation (in the center). Iron atoms in the outer green rings (2 nm thick) are kept fixed in order to permanently represent the correct displacement field created by the dislocations. (For interpretation of the references to color in this figure legend, the reader is referred to the web version of this article.)

be easily obtained in atomistic simulations by taking the difference between the total potential energies of a large simulation box with a carbon atom occupying either an O- or T-site and the same simulation box with no carbon. $E_{dislo}$, in turn, is the total potential energy of one of the simulation boxes depicted in Fig. 1. $E_{[O|T],carbon+dislo}$ refers to the total potential energy of the same simulation box with a single carbon atom in an O- or T-site. $E^b_{[O|T],atom} > 0$ reveals an attractive interaction between the point and the line defects, whereas $E^b_{[O|T],atom} < 0$ means that the dislocation repels the carbon atom.

The energy barrier of a transition along a specific minimum energy path is simply the difference between the total energy of the corresponding saddle point and the total energy of the current stable state. Therefore, regarding carbon migration from/to O-sites passing through a T-site in the neighborhood of a dislocation in α-iron, the energy barrier can be obtained, from atomistic simulations, by the following equation:

$$E^{eb}_{atom} = E_{T,carbon+dislo} - E_{O,carbon+dislo} \tag{2}$$

where $E_{T,carbon+dislo}$ and $E_{O,carbon+dislo}$ have the same meaning as in Eq. (1).

### 2.2. Elasticity calculations

In contrast with atomistic simulations, elasticity theory assumes a continuum description of a material. The underlying chemistry or other atomic properties of the host crystal which are not reflected in the elastic constants are not considered. In this work, the elastic constants of the bcc iron matrix corresponding to the Fe–Fe potential are $C_{11} = 243$, $C_{12} = 145$ and $C_{44} = 116$ GPa. Within elasticity theory, a point defect, such as carbon, is seen as a singular source of stress and modeled by its force moment tensor, also called the "elastic dipole", $P_{ij}$ [26].

As discussed in previous work [13], the elastic dipole $P_{ij}$ can be readily deduced from atomistic simulations by introducing the point defect in a simulation box of fixed volume $V$ with periodic boundary conditions in all directions, and then performing full coordinate optimization with a molecular statics algorithm (e.g. conjugate gradient). Elasticity theory then predicts that the homogeneous stress which develops in the simulation box varies linearly with the inverse of the volume through the following equation:

$$\sigma_{ij} = -\frac{1}{V} P_{ij} \tag{3}$$

Both the O- and T-interstitial sites have a tetragonal symmetry, with the tetragonal axis defined by the variant type. In the orientation given by $\vec{u}_x = (1,0,0)$, $\vec{u}_y = (0,1,0)$ and $\vec{u}_z = (0,0,1)$, the elastic dipole tensor $P_{ij}$ should therefore take the following form:

$$(P_{ij}) = \begin{pmatrix} P_{xx} & 0 & 0 \\ 0 & P_{yy} & 0 \\ 0 & 0 & P_{zz} \end{pmatrix}$$

with only two different diagonal terms ($P_{yy} = P_{zz}$ for instance for the [1 0 0] variant). As a consequence of Eq. (3), shear components of the stress tensor vanishes and the off-diagonal terms obey the same symmetry.

Fig. 2 presents $\sigma_{ii}(1/V)$ for a carbon atom in a [1 0 0] octahedral variant. The corresponding values of the non-zero components of the $P_{ij}$ tensor are $P_{xx} = 8.03$ eV and $P_{yy} = P_{zz} = 3.40$ eV. For the other two O-variants, the values of $P_{ii}$ are obtained by performing the appropriate permutations. In the same figure we can see also $\sigma_{ii}(1/V)$ for the [0 1 0] T-variant. In this case we have $P_{xx} = P_{zz} = 6.66$ eV and $P_{yy} = 4.87$ eV. Similar to the O-variants, the diagonal components of the $P_{ij}$ tensor must be permuted to find the ones corresponding to the other two T-variants.

From the $P_{ij}$ tensor associated with one of the interstitial sites, the corresponding relaxation volume $\Delta V$ of carbon in bcc iron within the elastic model is easily obtained by the following equation:

$$\Delta V_{[O|T]} = \frac{\mathrm{Tr}(P_{ij})}{C_{11} + 2C_{12}} \tag{4}$$

which results in $\Delta V_O = 0.0045$ nm$^3$ and $\Delta V_T = 0.0055$ nm$^3$. The migration volume $\Delta V_m = \Delta V_T - \Delta V_O = 0.001$ nm$^3$ compares well to the experimental data [27–29].

In the frame of anisotropic elasticity theory [30,31] with the formulation of the elastic dipole by Bacon and

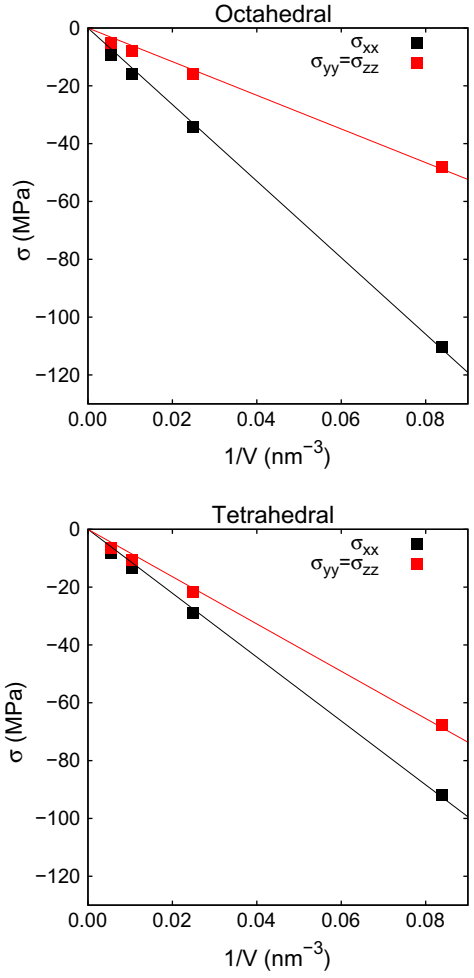


Fig. 2. Stress as a function of the inverse of the simulation box volume for a simulation box with a carbon atom sitting on either a [100] O-variant or a [010] T-variant. Symbols refer to atomistic simulation results and lines represent their linear regression.

co-authors [26], the binding energy between a point defect and a dislocation is obtained by the following equation:

$$E^{b}_{[O|T],elast} = P_{ij}\epsilon^{d}_{ij} \tag{5}$$

where $\epsilon^{d}_{ij}$ is the strain field of the dislocation at the location of the point defect [22,23]. After obtaining the binding energies for a carbon atom occupying an O- or a T-site with elasticity theory, the corresponding energy barrier can be obtained by rearranging Eq. (1):

$$E_{[O|T],carbon+dislo} = E_{[O|T],carbon} + E_{dislo} - E^{b}_{[O|T],elast} \tag{6}$$

and then taking the difference in Eq. (2):

$$\begin{aligned} E^{eb}_{elast} &= E_{T,carbon+dislo} - E_{O,carbon+dislo} \\ &= E_{T,carbon} + E_{dislo} - E^{b}_{T,elast} \\ &\quad - \left(E_{O,carbon} + E_{dislo} - E^{b}_{O,elast}\right) \\ &= E^{eb}_{bulk} - E^{b}_{T,elast} + E^{b}_{O,elast} \end{aligned} \tag{7}$$

where $E^{eb}_{bulk} = E_{T,carbon} - E_{O,carbon} = 0.816\,\text{eV}$ is the energy barrier for carbon migration in a non-strained iron matrix.

## 3. Results and discussion

### 3.1. Energy calculations with molecular statics

To perform the atomistic simulations, all the octahedral and tetrahedral sites within a radius of 6 nm around the dislocation line were first mapped. For every mapped interstitial site, a carbon atom was inserted in the corresponding position and the total energy of the system was obtained by performing conjugate gradient energy minimization (i.e. molecular statics). The total energies converged at about 1–2 meV, which means a tolerance in the atomic forces of less than $10^{-2}$ eV nm$^{-1}$. The system was fully relaxed with a carbon atom in an O-site. When occupying a T-site, the carbon atom was allowed to relax only on the plane perpendicular to the corresponding reaction coordinate. Throughout this work, the tetrahedral site has been assumed to be the saddle point whenever two neighboring energy minima have corresponded to the carbon atom sitting on octahedral sites. Minimum energy path calculations performed with the nudged elastic band (NEB) method have shown that taking the tetrahedral site (more precisely, the midpoint between two energy minima) as the saddle point for carbon migration is a good approximation even relatively near the dislocation lines (see Fig. 3).

Fig. 4 depicts a map of the energy barriers as a function of carbon position with respect to the dislocation line for the six types of transitions that a carbon atom can undergo in the vicinity of an edge dislocation. The first thing to notice is that the effect of the edge dislocation on the energy barriers is more pronounced running parallel to the glide plane, where the $\sigma_{xy}$ component of the dislocation stress tensor predominates. For the [1 0 0] and [0 0 1] O-site variants, in the simulation box orientation that we have adopted, the carbon atom induces a local shear of the two adjacent $(\bar{1}\,0\,1)$ planes, i.e. we have a local $\sigma_{xy} \neq 0$ which interacts with the long-range $\sigma_{xy}$ created by the edge dislocation. A carbon atom in a [0 1 0] O-site, in turn, induces a local $\sigma_{xz}$ shear. Since outside the core the $\sigma_{xz}$ component of the stress tensor of the edge dislocation vanishes, there is little interaction between the defects when a carbon atom lies on a [0 1 0] O-site near the glide plane. This explains the fact that energy barriers for transitions starting from a [0 1 0] O-site differ less from the bulk value than their counterparts. The largest variations in the migration energies occur when a carbon atom jumps between [1 0 0] and [0 0 1] O-sites near the glide plane. A carbon atom undergoing such transitions move on the $(\bar{1}\,0\,1)$ plane passing through a [0 1 0] T-site. Although less pronounced, there also are important variations in the migration energies just above and below the dislocation core, where the point and the line defects interact more owing to their corresponding normal stresses.

In contrast with the edge dislocation, the stress field of a screw dislocation is predominantly shear ($\sigma_{xz}$ and $\sigma_{yz}$), with a small normal contribution. The interaction of a carbon atom with a dislocation through their respective shear

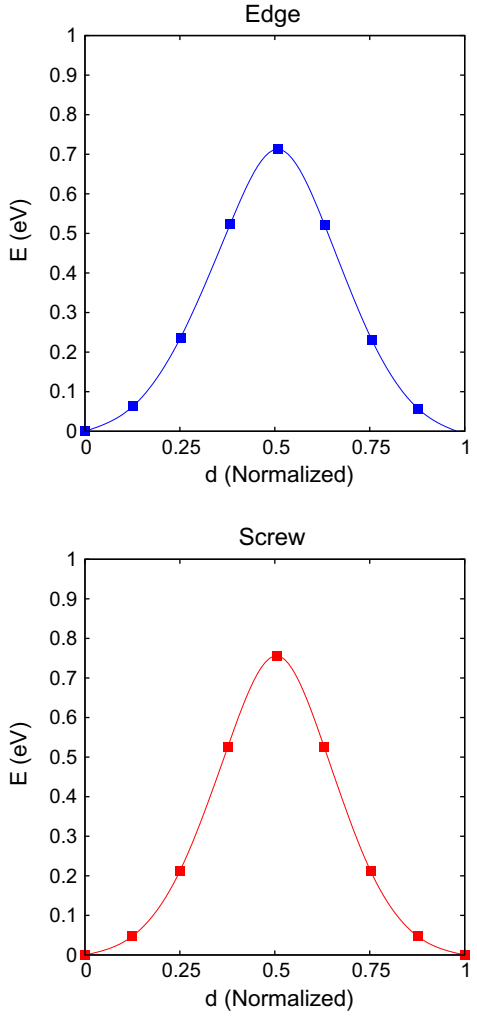


Fig. 3. NEB-calculated minimum energy paths for a carbon atom migrating between interstitial sites in the vicinity of either an edge or a screw dislocation. They refer to transitions between local energy minima found just above the dislocation cores ($x \approx 0$, $y \approx 0.6$–$0.7$ nm, with respect to the dislocation lines). In this plot, $d$ is the normalized distance between the two extremities of each path. The saddle points are found in the middle of the paths.

stresses is much more important when a carbon atom lies in an O-site than in a T-site, so that the energy barriers presented in Fig. 5 are mostly determined by the variation in the total energy of the carbon atom occupying an octahedral site. One can also see that the variation of the energy barriers for a given transition is mirrored by the variation of the energy barriers of the inverse transition. This draws an overall picture of the energy barriers for carbon migration around a screw dislocation which is much simpler than what is seen for an edge dislocation.

### 3.2. Comparison with elasticity calculations

#### 3.2.1. Differences in the migration energies

Anisotropic elasticity calculations have been carried out with the Babel code.[3] To perform the calculations, first the $P_{ij}$ tensors associated with the O- and T-sites were rotated according to the orientations shown in Fig. 1 in order to describe the local stress field of the carbon atom with respect to the dislocation line. Then the Volterra displacement field of either the edge or screw dislocation was applied to the positions of the interstitial sites found in a non-strained bcc iron lattice. $E^b_{O,elast}$ and $E^b_{T,elast}$ were calculated by using Eq. (5), and $E^{eb}_{elast}$ was obtained according to Eq. (7).

Absolute differences between the binding energies obtained by atomistic simulations and elasticity calculations can be seen in Figs. 6 and 7 for carbon positions around an edge and screw dislocation (i.e. $|\Delta E^b_{[O|T]}| = |E^b_{[O|T],atom} - E^b_{[O|T],elast}|$). Such differences represent the absolute errors that one should expect by replacing molecular statics by anisotropic elasticity theory. Not surprisingly, the agreement between the methods is much better when the carbon atom is closer to the screw dislocation than to the edge dislocation. A point raised by Ref. [13] helps to explain this discrepancy. In the elasticity calculations, only the Volterra displacement field of the dislocations has been taken into account. Nonetheless, the relaxation of the dislocation core and its surroundings with the current EAM potential yields an additional, shorter in range, displacement field. Considering that such a relaxation is larger for the edge dislocation compared to the screw dislocation, the resulting change of the dislocation stress field is also larger. For the T-sites, one can see that near the dislocation line the agreement is not as good as for the O-sites. We found a particularly noticeable discrepancy for the [0 1 0] T-site variant in the vicinity of the edge dislocation glide plane, for which elasticity theory predicts almost no interaction between the defects ($E^b_{T,elast} < 10^{-7}$ eV), in great contrast with atomistic simulations ($E^b_{T,atom}$ is in the order of $10^{-3}$ eV), so we have $|\Delta E^b_T| \approx |E^b_{T,atom}|$. The absolute error in this case is small simply because $|E^b_{T,atom}|$ is small. It should also be pointed out that, when a carbon atom in the glide plane of an edge dislocation reaches a point at a distance of approximately $3b$ from the dislocation line, both defects are seen to relax towards each other. Since carbon–dislocation separation is no longer the same as in elasticity calculations, no comparisons are made between the methods in this situation.

The absolute errors between energy barriers obtained by both methods are shown in Fig. 8. From a qualitative point of view, the energy barriers calculated by each method present the same trend and the relative errors in the energy barriers are usually very low (less than 5%). However, it is worthwhile pointing out that, in statistical mechanics, quantities that depend on migration energies (e.g. the probability of a carbon jump in bcc iron) are proportional to the Boltzmann factor $\exp(-E^{eb}/kT)$, where $k$ is the Boltzmann constant and $T$ is temperature. Consequently, because of the exponential, even small errors in the activation energies may yield large differences in the final results. For instance, if a threshold of about 20% is tolerated for the relative error in quantities determined by the Boltzmann factor at room temperature ($T = 300$ K), it means a maximum absolute

[3] Developed by E. Clouet at the CEA-Saclay.

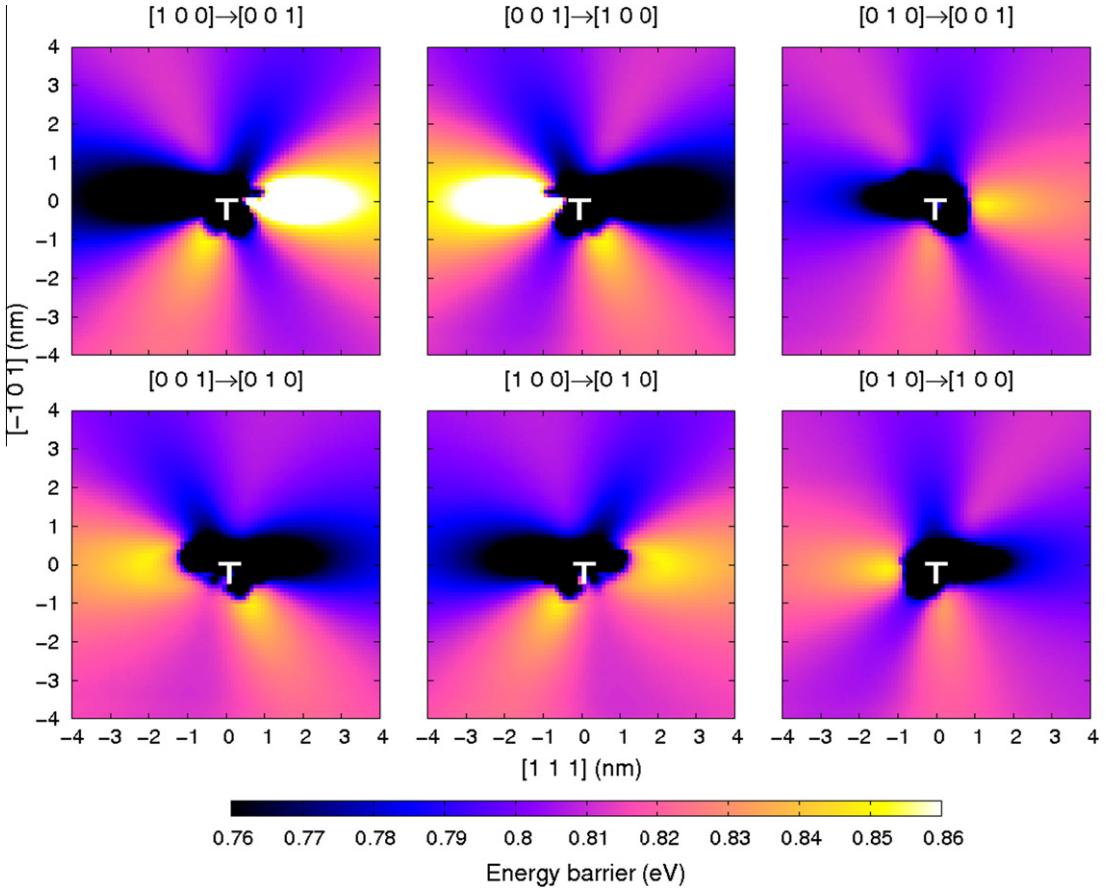


Fig. 4. Mapping of the energy barriers obtained by atomistic simulations for carbon migration in the vicinity of a straight edge dislocation (in the center) which is aligned parallel to the $[1\bar{2}1]$ direction (perpendicular to the page).

error of only 5 meV in the activation energies. This implies a minimum carbon–dislocation separation of about 1.5 nm for the screw dislocation and of about 2 nm for the edge dislocation (up to 4 nm in its glide plane).

### 3.2.2. Dislocation-induced bias on carbon diffusion

The stress field of an edge dislocation has been seen to induce a location-dependent bias on carbon diffusion [20] and this is expected also to be the case for a screw dislocation. Such a bias is quantified by the mean displacement vector $\langle\vec{d}\rangle$ [32], obtained as follows:

$$\langle\vec{d}\rangle = \sum_{j=1}^{N} P_{i\to j}\vec{\delta}_{i\to j} \tag{8}$$

where $\vec{\delta}_{i\to j}$ is the vector that connects $i$ to $j$ and $P_{i\to j}$ is the normalized probability to take the system from state $i$ to $j$, which is given by:

$$P_{i\to j} = \frac{\exp\left(-\frac{E^{eb}_{i\to j}}{kT}\right)}{\sum_{k=1}^{N}\exp\left(-\frac{E^{eb}_{i\to k}}{kT}\right)} \tag{9}$$

In our model, $N = 4$, as a carbon atom in an O-site can jump to one of its four neighboring O-sites. The vector $\langle\vec{d}\rangle$ points to the direction which a carbon atom passing in that specific location will take on average (after a large number of passages). The effect of the bias is therefore a drift on carbon trajectories, which do not spread isotropically in the strained iron lattice. In fact, if the bias is very strong, the carbon trajectory is less a random walk than an oriented one. It is also clear that the bias is stronger when the temperature is lower, tending to a simple (unbiased) random walk in the high temperature limit.

Figs. 9 and 10 allow the comparison of $\langle\vec{d}\rangle_{atom}$ and $\langle\vec{d}\rangle_{elast}$ around an edge and a screw dislocation, respectively, for $T = 300$ K (only vectors with a magnitude greater than $10^{-3}$ nm are shown). For the edge dislocation, both methods predict that a carbon atom above the glide plane tends to go to the dislocation core, underlining the attractive interaction between the defects in the part of the crystal under tension. On the other hand, below the glide plane (region under compression), the carbon atom tends to move obliquely with respect to the dislocation core towards the glide plane. For the screw dislocation, one can see that the bias is much less pronounced than in the edge case. Both methods reflect the effect of the threefold symmetry of the screw dislocation stress field on carbon diffusion, with attractive (repulsive) zones separated by 120°.

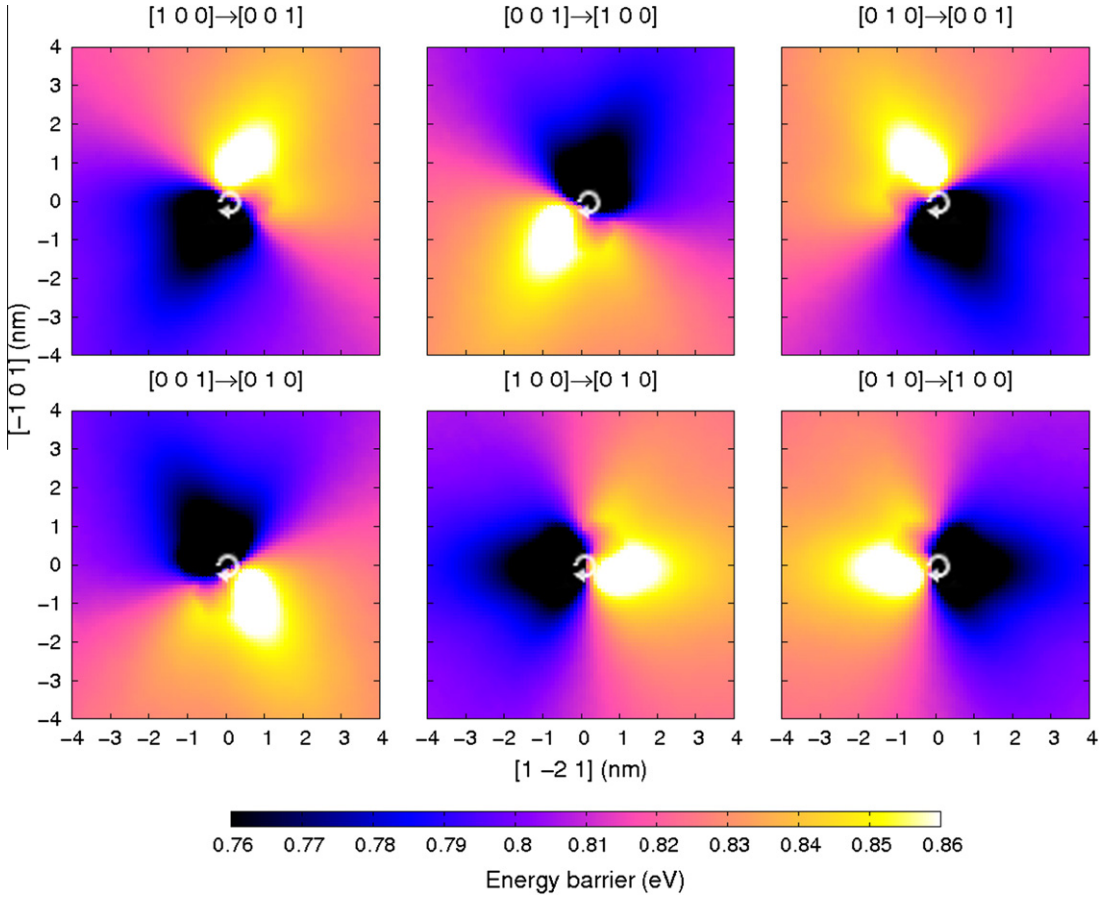


Fig. 5. Mapping of the energy barriers obtained by atomistic simulations for carbon migration in the vicinity of a straight screw dislocation (in the center) which is aligned parallel to the [111] direction (perpendicular to the page).

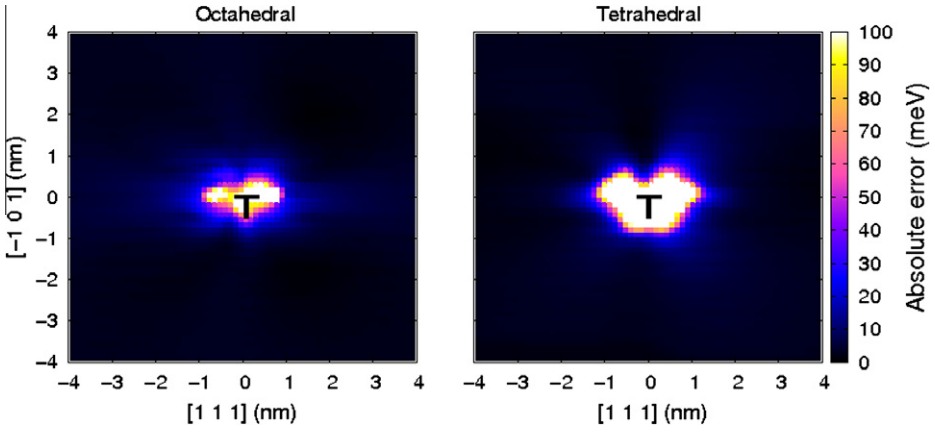


Fig. 6. Mapping of the absolute difference (error) $|\Delta E^{b}_{[O|T]}|$ between the binding energies obtained by atomistic simulations and anisotropic elasticity calculations as a function of carbon position around an edge dislocation (in the center).

## 4. Carbon segregation to dislocations

It is worthwhile evaluating the extent to which the differences in the activation energies might affect the simulated kinetics of carbon diffusion near a dislocation. For this purpose, we implemented the algorithm for atomistic kinetic Monte Carlo (AKMC) derived by Young and Elcock [7]. The AKMC simulation box consisted of a rigid lattice where every site corresponded to an O-site in the simulation box employed in atomistic simulations; it was thus also a cylinder of radius equal to 6 nm. For both dislocations, a core radius of $4b$ around the

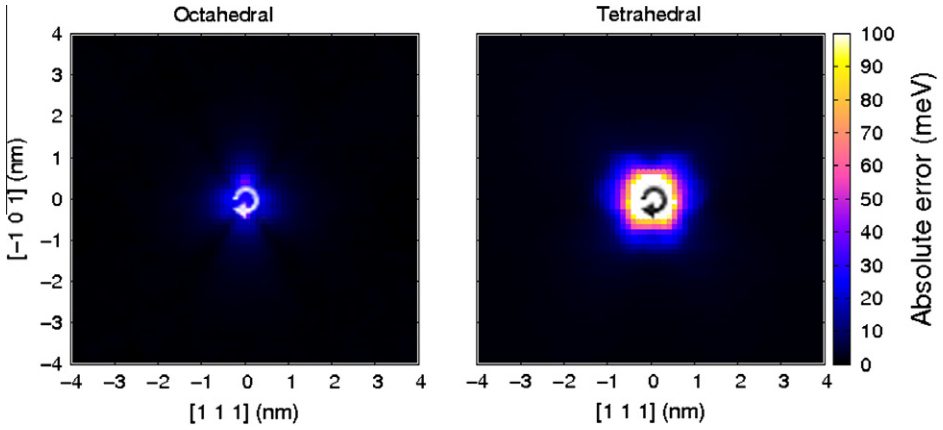


Fig. 7. Mapping of the absolute difference (error) $|\Delta E^{b}_{[O|T]}|$ between the binding energies obtained by atomistic simulations and anisotropic elasticity calculations as a function of carbon position around a screw dislocation (in the center).

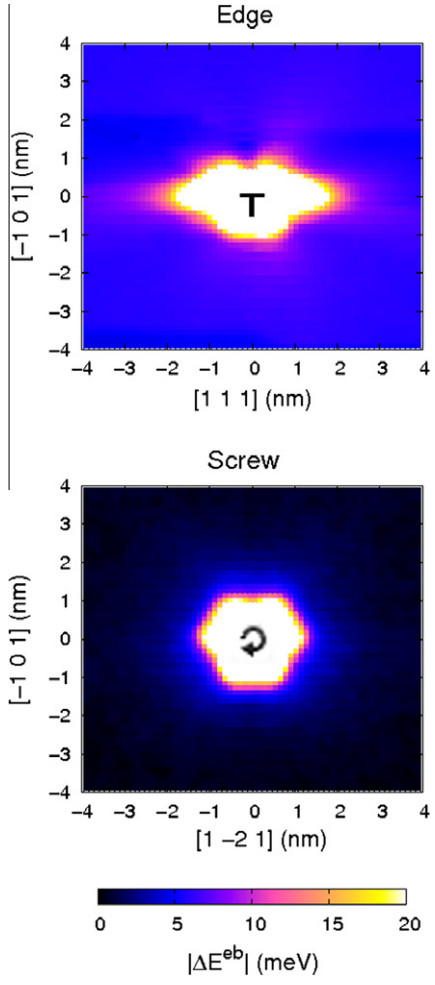


Fig. 8. Mapping of the absolute difference (error) $|\Delta E^{eb}|$ between the energy barriers obtained by atomistic simulations and anisotropic elasticity calculations as a function of carbon position around an edge or a screw dislocation (in the center). $|\Delta E^{eb}| > 5$ meV represents a relative error greater than 20% in quantities calculated by means of the Boltzmann factor at $T = 300$ K.

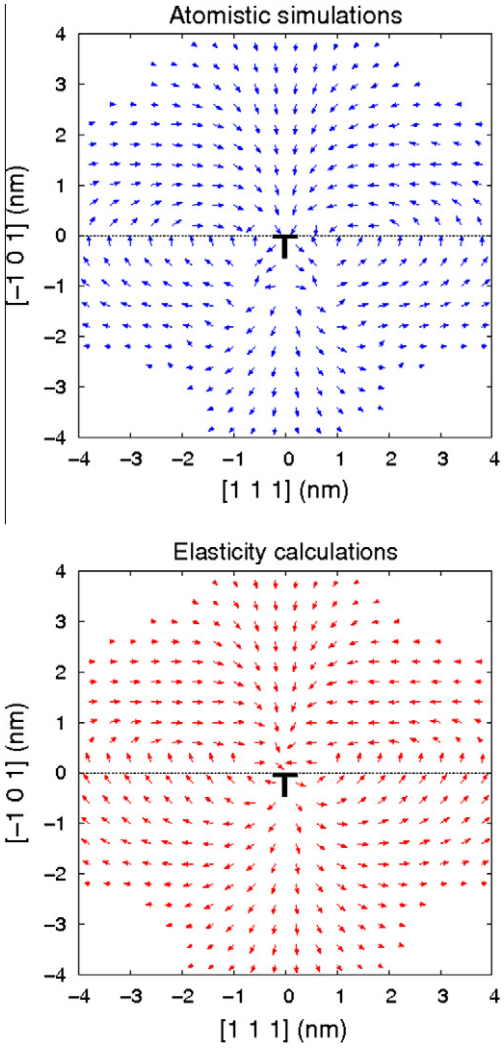


Fig. 9. Mean displacement vectors $\langle \vec{d} \rangle_{atom}$ and $\langle \vec{d} \rangle_{elast}$ in the vicinity of an edge dislocation at $T = 300$ K. Only vectors with lengths greater than $10^{-3}$ nm are plotted. For the sake of readability, the vectors were multiplied by 100. The $z$ component (parallel to the dislocation line) is not shown. Each arrow corresponds to the vector which is the resulting $\langle \vec{d} \rangle_{atom}$ or $\langle \vec{d} \rangle_{elast}$ in an area of $0.4 \times 0.4$ nm$^2$.

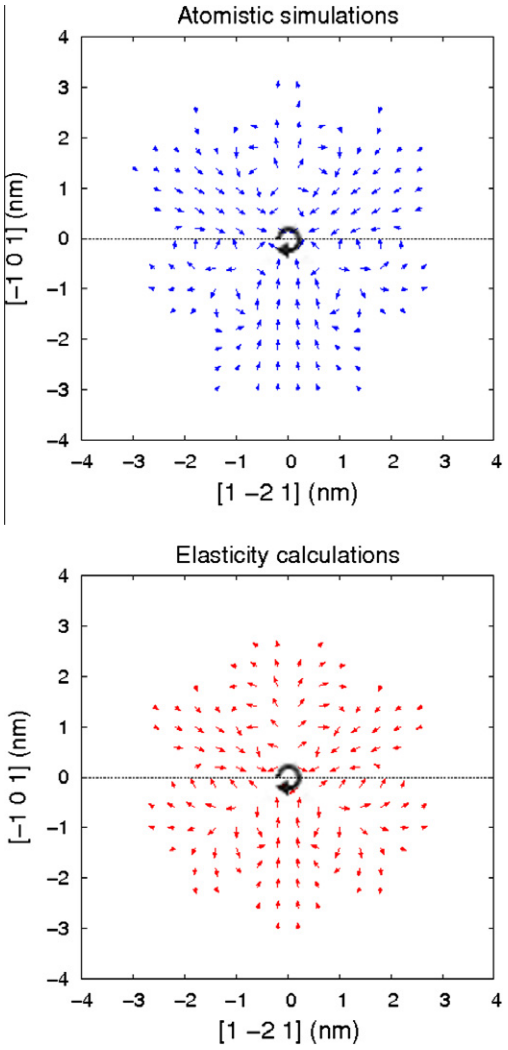


Fig. 10. Mean displacement vectors $\langle\vec{d}\rangle_{atom}$ and $\langle\vec{d}\rangle_{elast}$ in the vicinity of a screw dislocation at $T = 300$ K. Only vectors with lengths greater than $10^{-3}$ nm are plotted. For the sake of readability, the vectors were multiplied by 100. The $z$ component (parallel to the dislocation line) is not shown. Each arrow corresponds to the vector which is the resulting $\langle\vec{d}\rangle_{atom}$ or $\langle\vec{d}\rangle_{elast}$ in an area of $0.4 \times 0.4$ nm$^2$.

dislocation lines was defined ad hoc, where $b = |\vec{b}| \approx 0.25$ nm is the Burgers vector length. Sites encompassed by such a core radius and beyond the outer limit of the simulation box were considered as absorbing barriers (stop points) in the AKMC simulations. In the first case, a carbon atom is considered trapped by the dislocation; in the second case, the carbon trajectory is no longer followed. Each set of AKMC simulations generated 100,000 carbon trajectories, with a minimum of 100 and a maximum of 100,000 jumps at $T = 300$ K. This minimum number of jumps was chosen in order to prevent including in the statistics trajectories that either fall into the dislocation core or leave the simulation box through the outer boundary too quickly. Starting points were chosen at random and thus were equally distributed inside the simulation box, so that the resulting trajectories covered its whole volume and explored as many pathways as possible. Additionally, AKMC simulations were performed where the energy barriers were considered to be 0.816 eV everywhere. Comparison with the results of those simple (isotropic) random walks allows us to check the effect of the dislocation stress fields on carbon diffusion.

Owing to the boundary conditions, the kinetics of carbon segregation given by the AKMC simulations is a competition between the two absorbing barriers. Starting with the edge dislocation, atomistic simulations and elasticity calculations are in agreement when predicting the number of trajectories that ended in the dislocation core (about 34% vs. 27% of simple random walks). Thus the probability that a carbon atom will be trapped by the edge dislocation instead of leaving the simulation box is the same for both methods. The edge dislocation splits the simulation box into two different regions, one under tension and the other under compression (above and below the glide plane, respectively). We have seen that, irrespective of the method employed to obtain the migration energies, about 3/4 of the stress-assisted carbon trajectories that ended in the core of the edge dislocation started in the tension half. Moreover, considering only the carbon atoms trapped by the core whose trajectories started in the half under compression, more than 80% diffused first towards the glide plane before being led to the dislocation core. Therefore, it is very unlikely, according to either method, that a carbon atom will arrive at the core of an edge dislocation directly from the compression region. Unlike the edge dislocation, carbon trajectories generated from the atomistic-calculated migration energies have a higher probability to terminate in the screw dislocation core (32%) than the trajectories generated from elasticity results (29%).

We have also checked whether atomistic simulations and elasticity calculations yield similar kinetics of carbon segregation to dislocations. The evolution of the fraction of carbon atoms trapped by the edge or the screw dislocation is depicted in Fig. 11. The curves show the well-known sigmoidal shape usually reported in aging experiments [2,33,34]. There is also a delay in elasticity-informed AKMC simulations with respect to atomistic-informed ones that starts since the first carbon atoms are trapped by the dislocation. Those are generally the ones closest to the dislocation core, thus suggesting that this is a cumulative effect of the increasing absolute errors as the carbon atom approaches the sink.

Direct comparison of AKMC-simulated kinetics with aging experiments, while certainly desirable, is difficult, because the experimental length and time scale are usually much larger than what is possible to achieve with simulations. On the other hand, a bridge may be established through simple analytical kinetic models commonly used to describe the results of mechanical tests. In Hartley's model [35], for instance, the increase in yield strain during aging is assumed to be due only to dislocation locking by carbon. In other words, it is supposed to be proportional to carbon concentration on the dislocations. The kinetics of strain

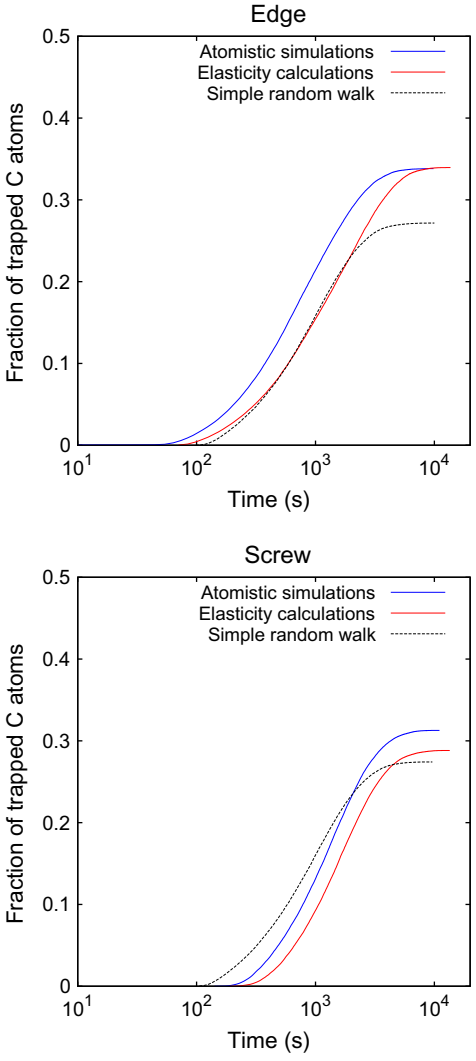


Fig. 11. Fraction of carbon trajectories that terminated in the core of either an edge or screw dislocation during AKMC simulations at $T = 300$ K.

aging from the measurement of changes in yield stress according to this model is given by the following equation:

$$\frac{\Delta\sigma}{\Delta\sigma_{max}} = c_1 + c_2(at)^n = c_1 + c_2\left(\frac{Dt}{T}\right)^n \quad (10)$$

where $\Delta\sigma/\Delta\sigma_{max}$ is the fractional increase in the yield stress during aging, $t$ is the aging time, $c_1$ and $c_2$ are constants that depend on the test conditions, $D$ is the diffusion coefficient, $T$ is temperature and $n = 2/3$. Deviations from 2/3 in the value of $n$ are usually associated with a change in the precipitation mechanism [36–38]. Indeed, experimental results reported by De and co-workers fitted to Hartley's model [34] show that the kinetics of aging in pre-strained ultra-low-carbon bake-hardening steels obey the $t^{\frac{2}{3}}$ kinetic law initially proposed in a lattice diffusion model by Cottrell and Bilby [1], thus indicating that dislocation densities up to a level of 10% pre-strain do not have an important effect on the kinetics. In our case, we assume in the following analysis that each AKMC simulation refers to the diffusion of a single carbon atom to a dislocation and that the ensemble of many simulations provides a picture of carbon segregation to line defects. This implies a low carbon concentration, so that every carbon trajectory is independent from the others and locks different segments of an infinitely long dislocation line. The simulation results were fitted to Eq. (10), with the fraction of carbon atoms trapped by the dislocation replacing $\Delta\sigma/\Delta\sigma_{max}$. Only the part of the curves before saturation in Fig. 11 (approximately the first 20 min) were considered in the fitting procedure. The kinetic parameters $n$ and $D = aT$ thus obtained are shown in Table 1. The deviations from the $t^{\frac{2}{3}}$ law are evident, but are still within the values experimentally found by Ref. [34]. Regarding the effective diffusion coefficient $D$, the value with the largest discrepancy (for the trajectories around an edge dislocation with energy barriers obtained by molecular statics) is of the same order of magnitude as the other values. Overall, these results show that, regardless of dislocation type (and, consequently, of the corresponding stress field) or method used to obtain the activation energies, trapping of carbon atoms by the dislocation proceeds according to the same kinetic law as $\Delta\sigma/\Delta\sigma_{max}$ during the first stage of static aging. This underlines the fundamental link between the microscopic phenomenon assessed by the AKMC simulations (carbon diffusion to a dislocation) and the change in the mechanical properties observed in the macroscopic experiments.

Table 1
Kinetic parameters obtained from AKMC simulations after fitting to Eq. (10).

| Dislocation | Method | $n$ | $D$ (m$^2$/s) |
|---|---|---|---|
| Edge | Molecular statics | 0.62 | $4.2 \times 10^{-21}$ |
| | Elasticity calculations | 0.66 | $2.5 \times 10^{-21}$ |
| | Simple random walk | 0.65 | $2.6 \times 10^{-21}$ |
| Screw | Molecular statics | 0.75 | $2.3 \times 10^{-21}$ |
| | Elasticity calculations | 0.70 | $1.7 \times 10^{-21}$ |
| | Simple random walk | 0.64 | $2.6 \times 10^{-21}$ |

The speed of a diffusional process in the solid state is related to the mean elapsed time $\langle\tau\rangle$ at every accessible state.[4] The mean elapsed time in a specific location $i$ is given by [5]:

$$\langle\tau\rangle = \frac{1}{\Omega_i} = \left[\nu_0 \sum_{j=1}^{N} \exp\left(\frac{-E^{eb}_{i\to j}}{kT}\right)\right]^{-1} \quad (11)$$

In this equation, one can see that $\langle\tau\rangle$ is the inverse of the sum of the transition rates $\Omega_i$; $\nu_0$ is the frequency of attempts ($10^{13}$ Hz). In Figs. 12 and 13, $\langle\tau\rangle$ obtained by atomistic simulations and elasticity calculations is shown as a function of carbon position with respect to the dislocation

[4] Indeed, the diffusion coefficient of an isotropic diffusional process (which we have shown is not the case for a carbon atom interacting with the stress field of dislocations), according to the well-known Einstein's formula, is: $D = \frac{1}{2d}\frac{\delta^2}{\langle\tau\rangle}$, where $d = 1,2,3$ is the dimension in which the diffusion occurs and $\delta$ is the jump distance.

lines at $T = 300$ K. For comparison, $\langle\tau\rangle \approx 1.25$ s for $E^{eb} = 0.816$ eV (simple random walk) and the same $\nu_0$. As can be seen, around an edge dislocation $\langle\tau\rangle_{atom}$ and $\langle\tau\rangle_{elast}$ exhibit the same trend: the carbon atom diffuses faster as it approaches the dislocation from the region under tension and slower from the region under compression or in the vicinity of the glide plane. On the other hand, the cumulative effect of the differences in the migration energies calculated by either method is also evident. The mean relative errors as a function of distance to the edge dislocation line between $\langle\tau\rangle_{atom}$ and $\langle\tau\rangle_{elast}$ reveal that elasticity calculations leads to an overestimation of the mean elapsed time (and, consequently, underestimation of the diffusivity) with respect to atomistic simulations of at least 20% (reaching to 50% near the core) within the maximum radius of 6 nm considered in this work. An interesting point is that the interatomic potential (and also elasticity) predicts that the carbon atom diffuses more slowly as it approaches the core of a screw dislocation, thus explaining the delay in stress-assisted trajectories with respect to simple random walks in Fig. 11. Disagreement between $\langle\tau\rangle_{atom}$ and $\langle\tau\rangle_{elast}$, in turn, becomes noticeable only when the carbon atom is about 2 nm away from the screw dislocation line.

## 5. Conclusions

Results have been presented for two different methods that can be applied to obtain carbon migration energies near dislocations in $\alpha$-iron. Atomistic simulations describe the Fe–C system as an ensemble of particles that interact with each other according to an interatomic potential – in this work, an EAM potential fitted to ab initio calculations. Anisotropic elasticity theory, in turn, considers a continuum medium distorted by the strain field of the line and point defects. Despite such an important difference, the methods agree reasonably well (absolute errors of less than 5 meV on average) if the carbon atom is far enough from the dislocation lines. However, it should be pointed out that even small absolute errors in the migration energies may lead to significative temperature-dependent errors in quantities that depend on the Boltzmann factor. Indeed, some important discrepancies have been found in AKMC simulations performed at $T = 300$ K, thus indicating that the atomistic treatment remains necessary when examining carbon behavior in the vicinity of the dislocation core, where errors due to the elasticity approximation are the largest.

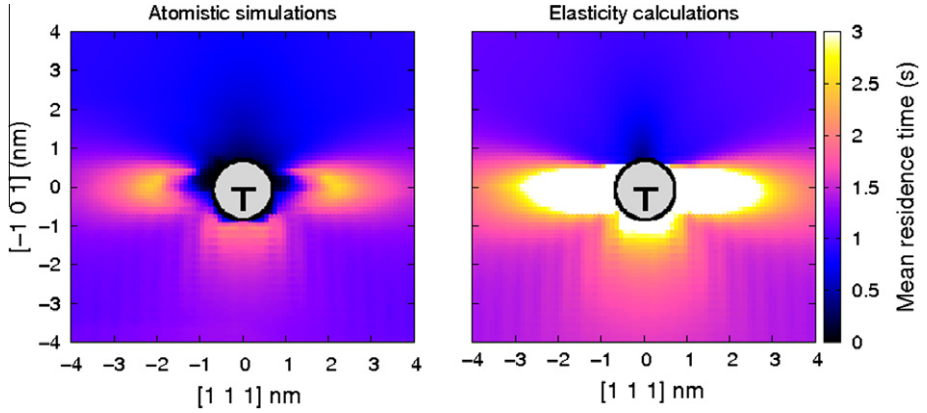


Fig. 12. Mapping of the mean elapsed times $\langle\tau\rangle_{atom}$ and $\langle\tau\rangle_{elast}$ at $T = 300$ K as a function of carbon position with respect to the edge dislocation line. The gray circle in the center (diameter equals to $8b$) refers to the region defined as the dislocation core in AKMC simulations.

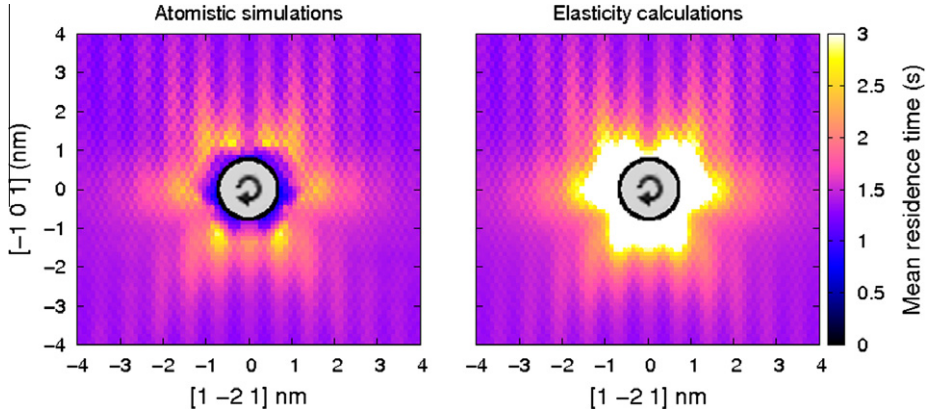


Fig. 13. Mapping of the mean elapsed times $\langle\tau\rangle_{atom}$ and $\langle\tau\rangle_{elast}$ at $T = 300$ K as a function of carbon position with respect to the screw dislocation line. The gray circle in the center (diameter equals to $8b$) refers to the region defined as the dislocation core in AKMC simulations.

In future work, atomistic simulations and anisotropic elasticity calculations may be incorporated into a single model using AKMC simulations to investigate the dynamics of Cottrell atmosphere formation in α-iron. Atomistic simulations should be restricted to the close vicinity of the line defects (2–4 nm away, depending on the acceptable error) and to situations where two or more carbon atoms are expected to interact with each other, whereas anisotropic elasticity should only be applied to the far-field.

## Acknowledgements

R.G.A.V. acknowledges EDF for funding. This work used computational facilities provided by P2CHPD cluster at Université Claude Bernard-Lyon 1 and the Centre Informatique National de l'Enseignement Supérieur (CINES). Partial support of "Agence Nationale de la Recherche" by CONTRAPRECI Project 06-BLAN-0205 and GraCoS Franco-canadian Project bl-inter09_483237-GraCoS is also gratefully acknowledged. This work was also supported by the European Commission in the framework of the PERFORM60 project under the grant agreement number 232612 in FP7/2007–2011. The authors also thank Drs. C.W. Sinclair and B. Lawrence (University of British Columbia, Canada) for critical reading of the manuscript.

## References

[1] Cottrell AH, Bilby BA. Proc Phys Soc A 1949;62:49.
[2] Lavaire N, Merlin J, Sardoy V. Scripta Mater 2001;44:554.
[3] Kubin LP, Estrin Y. Acta Metall 1983;41:397.
[4] Belotteau J, Berdin C, Forest S, Parrot A, Prioul C. Mater Sci Eng A 2009;526:156.
[5] Voter AF, Montalenti F, Germann TC. Ann Rev Mater Res 2002;32(1):321–46. doi:10.1146/annurev.matsci.32.112601.141541.
[6] Fichthorn KA, Weinberg WH. J Chem Phys 1991;95:1090.
[7] Young WM, Elcock EW. Proc Phys Soc 1966;89:735.
[8] Bortz AB, Kalos MH, Lebowitz JL. J Comp Phys 1975;17:10.
[9] Marcelin R. Ann Phys 1915;3:120.
[10] Wigner E. Z Phys Chem 1932;19:203.
[11] Eyring H. J Chem Phys 1935;3:107.
[12] Clouet E. Acta Mater 2006;54:3543.
[13] Clouet E, Garruchet S, Nguyen H, Perez M, Becquart CS. Acta Mater 2008;56:3450.
[14] Hanlumyuang Y, Gordon PA, Neeraj T, Chrzan DC. Acta Mater 2010;58:5481.
[15] Plimpton SJ. J Comp Phys 1995;117:1.
[16] Daw MS, Baskes MI. Phys Rev Lett 1983;50:1285.
[17] Becquart CS, Raulot JM, Benecteux G, Domain C, Perez M, Garruchet S, et al. Comp Mater Sci 2007;40:119–29.
[18] Ackland GJ, Mendelev MI, Srolovitz DJ, Han S, Barashev AV. J Phys: Condens Mater 2004;16:S2629.
[19] Garruchet S, Perez M. Comput Mater Sci 2008;43(2):286–92.
[20] Veiga RGA, Perez M, Becquart CS, Domain C, Garruchet S. Phys Rev B 2010;82:054103.
[21] Eshelby JD, Read WT, Shockley W. Acta Metall 1953;1:251.
[22] Stroh AN. J Math Phys 1962;41:77.
[23] Stroh AN. Philos Mag 1958;3:625.
[24] Porter DA, Easterling KE. Phase transformations in metals and alloys. 2nd ed. London: Chapman & Hall; 1981.
[25] Jiang DE, Carter EA. Phys Rev B 2003;67:214103.
[26] Bacon DJ, Barnett DM. Scattergood RO. Prog Mater Sci 1980;23:51.
[27] Wuttig M, Keiser J. Phys Rev B 1971;3:815.
[28] Bosman AJ, Brommer PE, Eijkelenboom LCH, Schinkel CJ, Rathenau GW. Physica 1960;26:533.
[29] Bass J, Lazarus D. J Phys Chem Solids 1962;23:1820.
[30] Eshelby JD. Acta Metall 1955;3:487.
[31] Douthwaite RM, Evans JT. Scripta Metall 1973;7:1019.
[32] Barlett VR, Bigeón JJ, Hoyuelos M, Mártin HOM. J Comp Phys 2009;228:5740.
[33] Lavaire N, Massardier V, Merlin J. Scripta Mater 2004;50:131.
[34] De AK, Vandeputte S, Cooman BCD. JMEPEG 2001;10:567.
[35] Hartley S. Acta Metall 1966;14:1237.
[36] Leslie WC. Acta Metall 1961;9:1004.
[37] Bullough R, Newman RC. Proc Roy Soc A 1959;249:427.
[38] Buono VTL, Andrade MS, Gonzalez BM. Metall Trans A 1998;29A:1415.